Enhancement of punching shear behavior of reinforced concrete flat slabs using GFRP grating

Haitham M.F. Mostafa, Ahmed A. Mahmoud, Tarek S. Mustafa, Ahmed N. M. Khater
Benha University, Faculty of Engineering at Shoubra, Civil Engineering Department, 108 Shoubra Street, Shoubra 11691, Cairo, Egypt
haiythaam@yahoo.com, https://orcid.org/0009-0004-2287-7564
ahmed.ahmed@feng.bu.edu.eg, http://orcid.org/0000-0003-2306-5950
Tarek.mohamed@feng.bu.edu.eg, http://orcid.org/0000-0002-0015-9113
ahmed.khater@feng.bu.edu.eg, http://orcid.org/0000-0003-4528-8979

Citation: Mostafa, H.. M. F., Mahmaoud, A. A., Mustafa, T. S., Khater, A. N. M., Enhancement of punching shear behavior of reinforced concrete flat slabs using GFRP grating, Frattura ed Integrità Strutturale, 68 (2024) 19-44.

Received: 31.08.2023
Accepted: 31.12.2023
Published: 12.01.2024
Issue: 04.2024

KEYWORDS. Punching shear, GFRP grating; RC flat slab, Numerical analysis, Experimental investigation, Code provisions.

INTRODUCTION

In recent years, the use of Fiber-Reinforced-Polymer (FRP) as an alternative reinforcing material in reinforced concrete structures has developed as a new solution to the corrosion problem. In addition to being non-corrosive, FRP materials have a high strength-to-weight ratio, are lightweight, have high tensile strength, and can be fabricated in various shapes, making them an attractive choice as a reinforcing material for concrete flat slabs.

Several studies investigating the influence of FRP resistance on the punching shear of RC flat slabs have been conducted. Swamy and Ali [1] studied the effect of fiber on deflection, strength properties, and punching shear failures. The fibers were

used throughout the slab or in the punching shear region of the column head, and comparative tests on connections with bending steel bars were performed. The fibers reduce deformations, increase ultimate punching shear loads, and transform failures from brittle to ductile. Results demonstrated that 1% fiber volume decreases deflections by 30% and enhances ductility and energy absorption. Ospina et al. [2] performed experiments to explore the use of FRP reinforcement in concrete slabs, comparing its behavior with traditional steel reinforcement. Ospina et al. [2] test results indicated that FRP-reinforced slabs do not experience punching shear failure triggered by FRP rupture, even with lighter reinforcement. The proposed equations address the unique characteristics of FRP reinforcement, as existing standards may not directly apply due to variations in elastic stiffness. Mu and Meyer [3] investigated experimentally the effect of fiber-reinforced glass bars in concrete slabs exposed to a central patched load. Results indicated that fiber mesh is more effective in bending, while randomly distributed fibers are somewhat better at punching shear. The critical punching shear perimeter is unaffected by fiber type, form, and volume ratio. Crushed glass aggregate influences slab strength and failure mode, but concerns about long-term alkali-silica reactions have been addressed. Zhang et al. [4] compared the results of three specimens of one-way concrete slab reinforced with CFRP grid reinforcement in addition to a specimen reinforced with steel bars. Findings indicated that higher CFRP reinforcement ratios are needed for sufficient flexural stiffness, and the Tureyen–Frosch shear equation is proposed for predicting the ultimate moment in FRP-reinforced slabs. Dimitrios et al. [5] predicted analytically the ultimate strength of fiber-reinforced polymer (FRP)-reinforced structural elements like flat slabs and bridge decks. The analytical model, validated with experimental data for FRP-reinforced slabs, offers a reliable framework for punching shear strength analysis, emphasizing the importance of knowing FRP bonding characteristics. Esfahani et al. [6] investigated the punching shear strengthening of flat slabs using Carbon-Fiber-Reinforced-Polymer (CFRP) sheets. Results show significant enhancement, especially for high-strength concrete with low steel reinforcement, but under cyclic loading, the effect diminishes. Stuart et al. [7] explored FRP rebar for concrete reinforcement, particularly in slabs, evaluating performance based on ACI, CSA, and Eurocode standards. Findings revealed variations in code accuracy, emphasizing the need for additional research to enhance the safety of FRP-reinforced concrete design. Abdulrahman et al. [8] studied experimentally and numerically strengthened flat slab-to-column corner connections with and without openings using CFRP sheets. The findings indicated that strengthening increased punching shear capacity by 11% for slabs without openings and up to 23% for slabs with openings. Hemzah et al. [9], investigating the punching shear performance of ten slab specimens considering variations in shape, reinforcement types (steel or CFRP), ratios, and the impact of double-layer reinforcement, highlighted that factors such as compressive strength and column shape significantly influence punching shear strength. A proposed formula, considering reinforcement type, ratio, concrete strength, and double-layer effect, showed good agreement with experimental results and existing codes. Said et al. [10] conducted an experimental and numerical program for thirteen lightweight concrete flat slab specimens to improve the punching shear resistance by using different strengthening techniques. The most effective method, radial shear reinforcement with (d/2) spacing, significantly improves punching shear capacity (77% with steel bars, 61% with glass fiber rods, and 54% with high-strength bolts). Kim and Lee [11] investigated the structural behavior of reinforced concrete flat slabs shear reinforced with GFRP vertical grids. Results from experiments showed increased shear strength with more and closer shear reinforcement. GFRP changed failure modes from brittle punching to flexure. Comparison with design codes revealed underestimation, with BS 8110 showing reasonable accuracy, emphasizing the effectiveness of GFRP in resisting punching shear.

Otherwise, few studies have been conducted on FRP with grating-shaped performance characteristics and its effectiveness as a punching shear resistance. Full-scale studies on a concrete slab bridge deck strengthened with pultruded glass fiber gratings were conducted by Bank et al. [12]. The results comply with AASHTO recommendations. The investigation shows that FRP gratings could be viable reinforcements, providing reasonable deflections and load capacities over three times the service load, with failure modes distinct from steel-reinforced slabs. Bank et al. [13] conducted experimental and analytical research to investigate the influence of pultruded FRP grating cages on reinforced concrete beams, comparing their performance to a steel-reinforced control beam. The results and failure modes are detailed, with a proposed analytical model predicting failure loads and deflection at failure. The study suggests the potential for using FRP grating cages for concrete reinforcement in construction. Biddah [14] investigated the use of pultruded GFRP grating sections as structural reinforcement for bridge decks in place of steel reinforcement of concrete slabs. The grating significantly increases capacity and flexural stiffness, showing potential as an economical alternative for bridge deck construction, offering high strength, easy installation, and preventing local buckling failure. Devender et al. [15] investigated experimentally the mechanical and chemical characteristics of GFRP grating. The composite grating, formed by resin and fiberglass, undergoes tests and is chosen over mild steel due to its durability, rust-free nature, and cost-effectiveness. Gattescoa et al. [16] discussed experimental bending tests on full-scale, molded FRP grating, exploring varied support conditions and the influence of FRP covers on stiffness and resistance. Rib collaboration enhances load capacity, while improving performance may lead to premature failure.

This research investigates the enhancement of punching shear resistance in flat slab-column connections using molded GFRP grating. This FRP type finds versatile applications, providing non-slip surfaces for walkways and platforms and excelling in corrosive environments like chemical plants. The ordered fiber arrangement boosts its strength, making molded GFRP gratings reliable for various structural components while maintaining their lightweight nature. Experimental testing, including varying parameters such as grating location, number, thickness, and size, has been performed. Additionally, a numerical model was developed for an extensive parametric study, with the results systematically compared to established structural design codes.

METHODOLOGY

Experimental program

Seven square slab column specimens measuring 1100×1100 mm with a thickness of 150 mm designed to fail in punching were cast and tested in the concrete laboratory at Cairo University's Faculty of Engineering. The column was cast monolithically at the specimen's center with a 300-mm square section, and its height is 300 mm. The main steel reinforcement of the slab is regularly spaced using 5 ϕ 16 mesh as a bottom tension reinforcement and 5 ϕ 12 mesh as a top compression reinforcement. The column reinforcement is 8 ϕ 12 with 8 mm stirrups each 100 mm. Figs. 1 to 3 showed typical concrete dimensions, photographs, and steel reinforcement for the tested specimens. The specimens were divided into five groups to investigate the studied parameters. The first group comprises two specimens, SP01 without gratings and SP02 with GFRP gratings, with sizes 700×700×15 mm placed in the mid-slab thickness to explore the effect of the new suggested gratings on punching shear performance. The second group includes three specimens (SP02, SP03, and SP04) with GFRP gratings 700×700×15 mm at the middle, top, and bottom of the slab thickness to study the influence of gratings position across the slab thickness. The third group consists of two specimens (SP02 and SP05) to study the influence of the number of gratings, where specimen SP02 has a single 700×700×15 mm GFRP grating located at the mid-slab thickness, whereas specimen SP05 has two GFRP gratings of the same dimensions connected to the top and bottom reinforcing steel of the specimen. Specimens SP02 and SP06 in the fourth group contain identical 700×700 mm GFRP grating with thicknesses of 15 and 38 mm, respectively, to study the effect of grating thickness. The fifth group includes two specimens, SP02 and SP07, with different GFRP grating dimensions of 700×700×15 mm and 800×800×15 mm, respectively, to investigate the effect of grating dimensions. Tab. 1 summarizes the studied parameters.

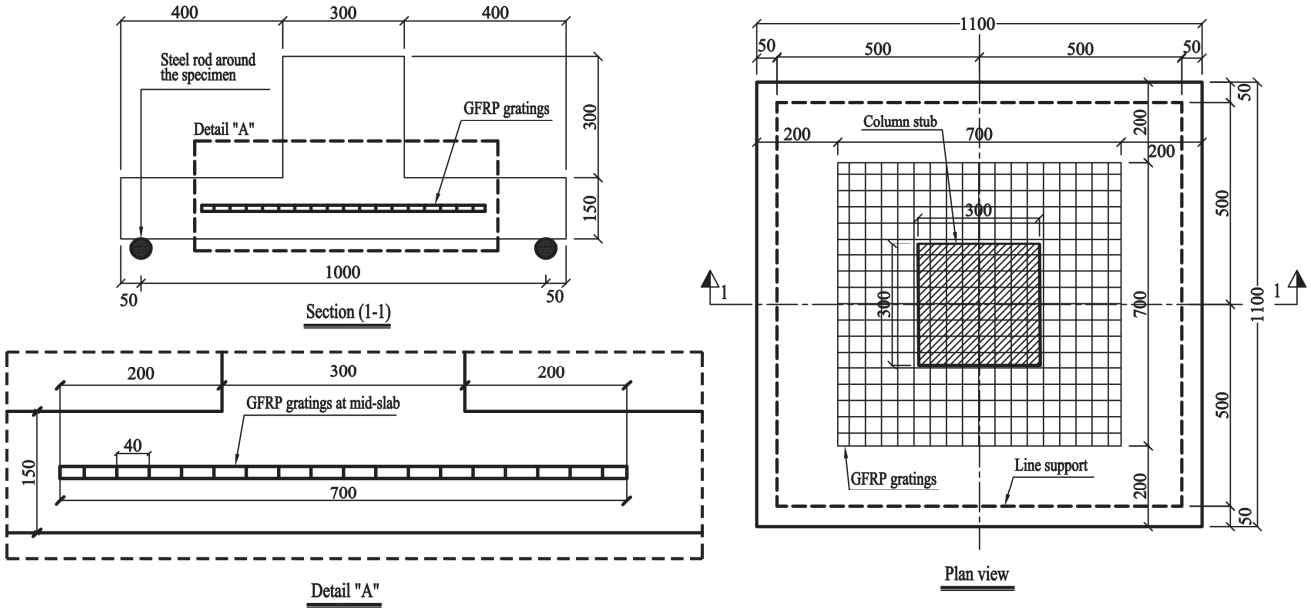

Figure 1: Typical concrete dimensions for the tested specimens

Figure 2: Tested specimen's preparation, reinforcement, and cast.

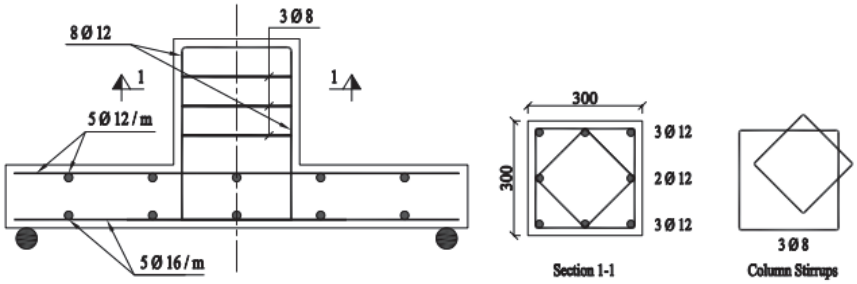

Figure 3: Typical reinforcement details for the tested specimens.

Specimen model	Group No.	GFRP grating dimensions (mm)	Grating position through the slab thickness	Number of gratings	Grating thickness (mm)	Notes
SP01	Control specimen	Without gratings	Without gratings	-	Without gratings	Control specimen
SP01	1	Without gratings	Without gratings	-	Without gratings	Effects of using the grating
SP02		700x700	Middle	1	15	
SP02		700x700	Middle	1	15	Effect of grating position on the slab thickness
SP03	2	700x700	Bottom	1	15	
SP04		700x700	Top	1	15	
SP02	3	700x700	Middle	1	15	Effect of the number of gratings
SP05		700x700	Top and bottom	2	15	
SP02	4	700x700	Middle	1	15	Effect of grating thickness
SP06		700x700	Middle	1	38	
SP02	5	700x700	Middle	1	15	Effect of grating dimensions
SP07		800x800	Middle	1	15	

Table 1: Studied parameters.

Mixture composition, material properties, and test setup

The experimental program used locally sourced crushed brown dolomite as coarse aggregate and sand as fine aggregate. In all mixes of the tested slabs, the ratio of fine to coarse aggregate was determined to be 1:1.65 (by weight). Ordinary Portland Cement (OPC) is made locally and according to Egyptian standard specifications, ECP 203 [17]. American Code ACI 318 2019 [18] was utilized in this investigation. For the mixing and curing of concrete, clean, drinkable water devoid of contaminants was utilized. The water-cement ratio of 0.54 (by weight) was specified. ASTM [19- 21] was used to find the experimental data for the used concrete and steel reinforcement. The average concrete strength after 28 days on the testing day was 25 MPa. Fig. 4.a shows the stress-strain curve for concrete. Deformed high-tensile steel bars with diameters of 12 mm and 16 mm and yield and ultimate strengths of 486, 579 MPa, and 444, 553 MPa, respectively, were recorded. Fig. 4.b presents the stress-strain curve for the reinforcing steel bars.

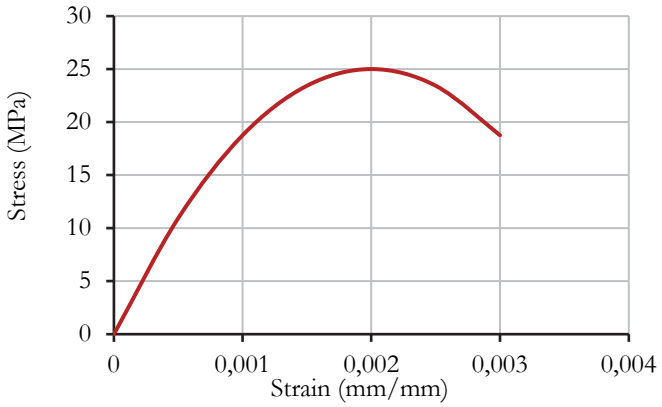

(a) Stress-strain curve for concrete according to ASTM 370-17 [20]

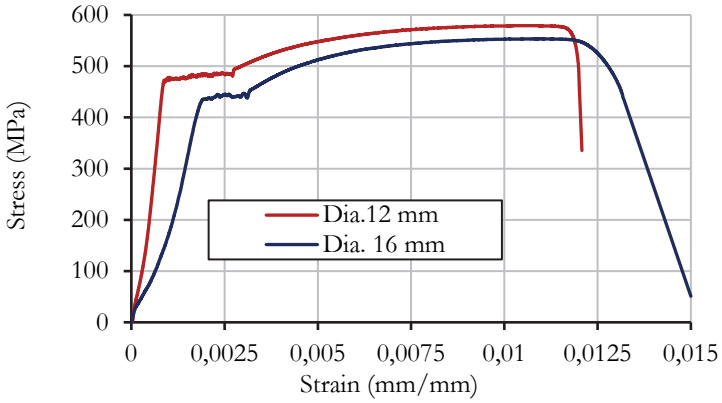

(b) Stress-strain curves for the used steel bars (according to ASTM C39/C39M-21[19]

Figure 4: Stress-strain curves for concrete and the used steel bars

To find experimental data on the GFRP grating, seven molded GFRP gratings were obtained from the Egypt FRP composite factory according to ECP-208 [22] with varying thicknesses, as shown in Fig. 5. Two grating specimens with dimensions of 200×1000×15 mm and 500×500×38 mm were tested according to ASTM D790-02 [23], where they were subjected to a central line load to figure out the central deflection as well as the strain that would occur for each grating and evaluate the elastic modulus. The central deflection was measured by LVDT, and strain gauges were employed to monitor the grating strain. According to the data, the elastic modulus of grating with thicknesses of 38 mm and 15 mm is 12 GPa and 6 GPa, respectively. Figs. 6 and 7 illustrate the experimental setup and stress-strain curves for both grating specimens. Fig. 8 shows the standard test setup. One load cell with a capacity of 1000 kN was used to apply the load. The specimens were supported on their four sides on steel rods with a 25-mm diameter. The load was applied as a monotonic static load using displacement control. At each load increment, cracks were identified. Electrical strain gauges were used to measure the strains in concrete, in the tension reinforcement, and in the GFRP gratings.

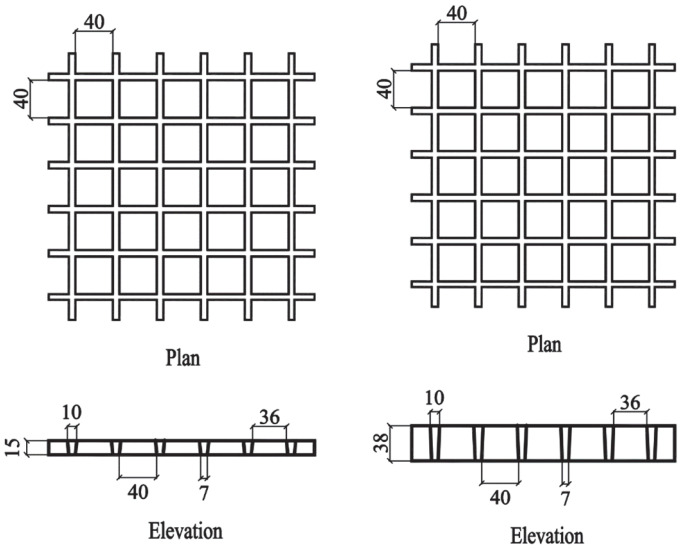

(a) 15 mm thickness (b) 38 mm thickness

Figure 5: Dimensions of grating with thicknesses of 15 and 38 mm.

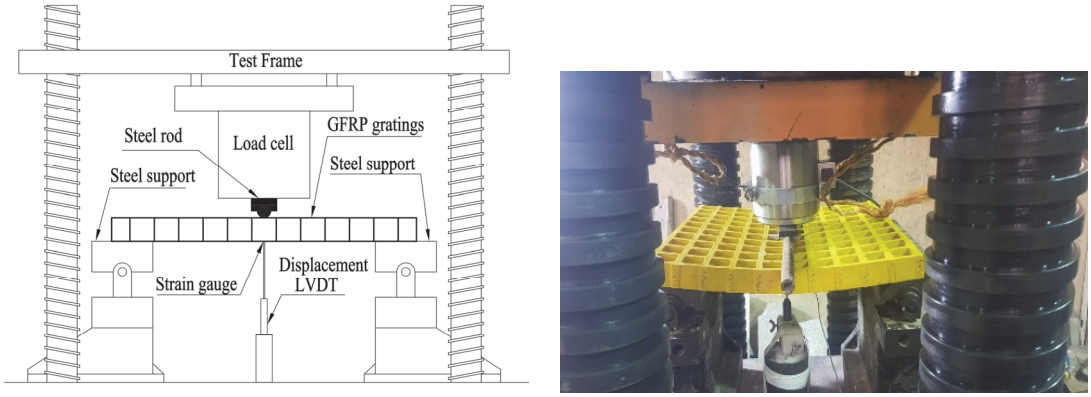

Figure 6: Test setup for GFRP gratings.

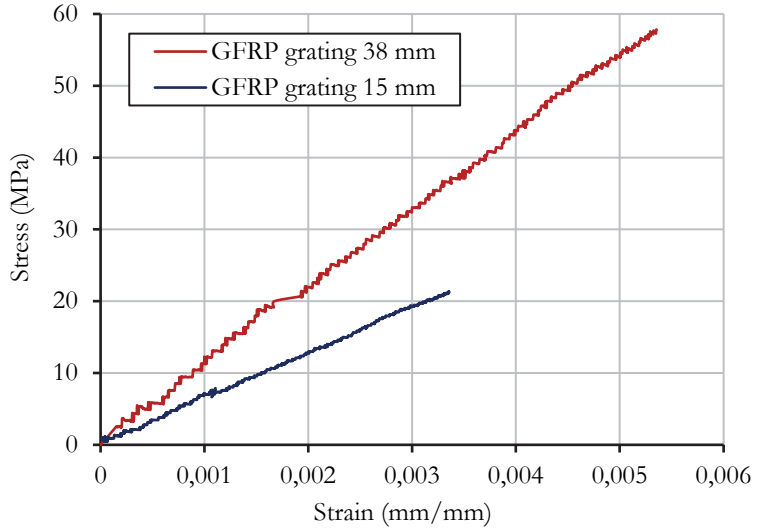

Figure 7: Stress-strain curves for the used GFRP gratings ASTM D790-02 [23].

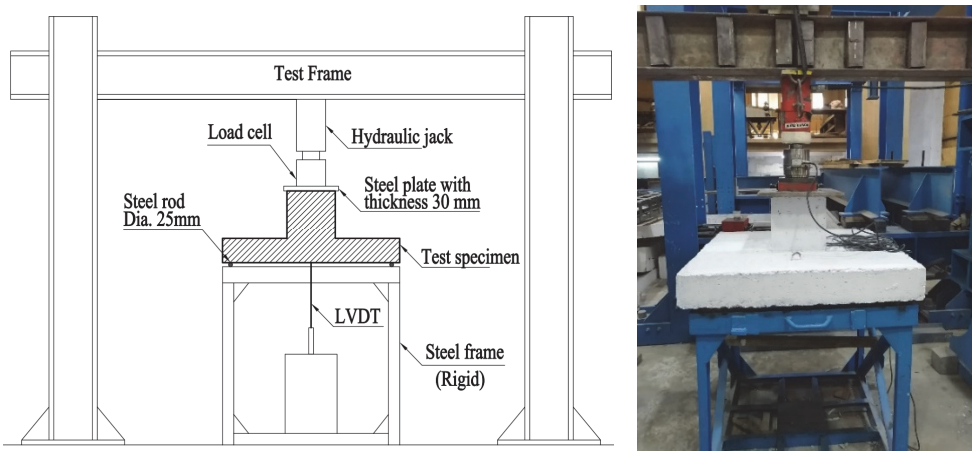

Figure 8: Test setup.

Numerical analysis

A nonlinear finite element analysis (NLFEA) using the ANSYS R15.0 [24] software package and a comparison of experimental and numerical results are presented. Correlational investigations based on the load-deflection response, crack patterns, and failure modes were employed to verify the numerical model results against the experimental results. The concrete element was modeled using a three-dimensional isoparametric element, Solid 65, while the steel reinforcement and GFRP gratings were modeled using the Link 8 element, which has two nodes with three degrees of freedom in translation at each node in the X, Y, and Z axes. It is assumed that the bond between steel reinforcement, GFRP gratings, and concrete is the perfect bond. Setting the boundary condition was simple; the Y translation degree of freedom was constrained at all nodes along the support line, and the X and Z translation degrees of freedom were constrained at the center nodes along the support line edges parallel to the Z axis and X axis to prevent the slab from sliding in its plane.

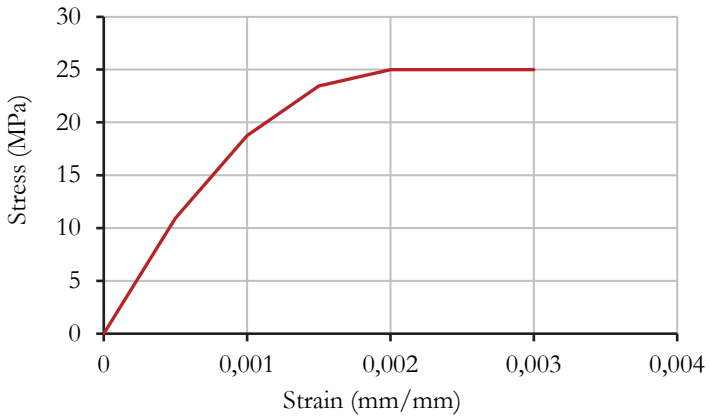

Figure 9: Idealized stress-strain curve for concrete in compression.

Material modeling

Fig. 9 demonstrates utilized idealized stress-strain relationship for concrete in compression. The modulus of elasticity of concrete (E_c) was determined by Martinez et al. [25] as Eq. (1). Fig. 10 displays a bilinear stress-strain curve with two straight branches, which represents the idealized behavior of the steel reinforcement. The relationship between the two segments of the line is characterized by Eqns. (2) and (3), where: ε_u is the ultimate strain of the steel reinforcement and equals 10 ε_y; f_u is the ultimate strength of the steel reinforcement relating to the ultimate strain ε_u; and E_s is the elastic modulus of the reinforcing steel. The steel reinforcement's elastic modulus E_s was taken to be 200000 MPa, and E_h is the elastic modulus at the second branch of the curve indicating the strain hardening region and was taken to be 0.1 E_s. As illustrated in Fig. 11, the GFRP gratings stress-strain curve is linear until failure, where f_{gu} is the ultimate strength of the GFRP gratings, ε_{gu} is the ultimate strain, and E_g is the modulus of elasticity of the GFRP gratings, which is equal to f_{gu}/ε_{gu}.

$$E_c = 3320 f_c'^{1/2} + 6900 \quad (\text{MPa}) \tag{1}$$

$$f_s = E_s \varepsilon_s \qquad \varepsilon_s \le \varepsilon_y \tag{2}$$

$$f_s = f_y + E_h \left(\varepsilon_s - \varepsilon_y \right) \qquad \varepsilon_y < \varepsilon_s \le \varepsilon_u \tag{3}$$

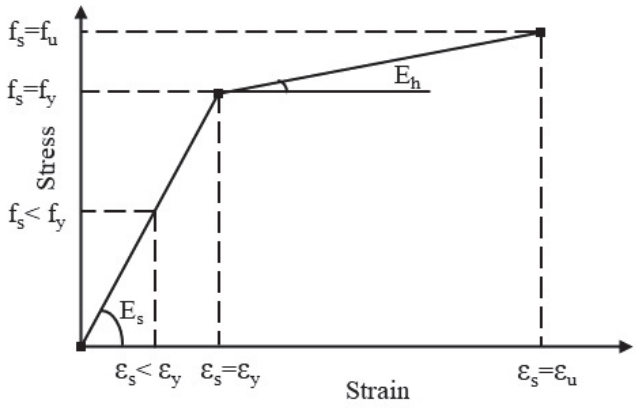

Figure 10: Bilinear stress-strain curve for steel reinforcement.

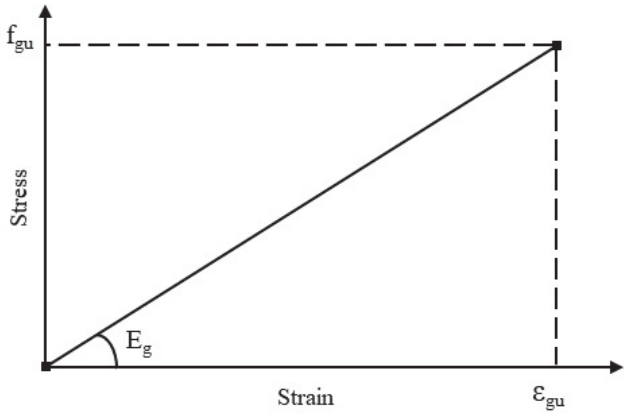

Figure 11: Stress-strain curve for GFRP gratings.

Solution techniques

It is generally agreed that the shear transfer coefficient for a closed crack (β_c) lies between 0.8 and 0.9; however, the shear transfer coefficient (β_t) used in this investigation was set at 0.2. The numerical solution scheme incorporated a load increment procedure to account for the nonlinear analysis. Each load increment was solved using an iterative process that combined the high convergence rate of the standard Newton-Raphson method with the low cost of the modified Newton-Raphson strategy, in which the stiffness is reformulated at each loading step as used by Mahmoud [26]. The convergence criterion relied on iterative nodal displacement, and only transitional degrees of freedom were considered. For this criterion: $\psi / R \le \phi$, we need to know the iterative displacement norm (ψ) and the total displacement norm (R). Satisfactory outcomes were observed within the convergence tolerance (ϕ) range of 0.02 to 0.05. The numerical ultimate load of the test specimen was determined to be the load at which numerical instability occurred due to a failure of the convergence condition.

Validation model

Fig. 12 shows the conventional 28×28×6 mesh of three-dimensional isoparametric elements, Solid 65, used to characterize all tested specimens. Six layers of elements were employed to determine the optimal thickness of the slab. The top and bottom layers represent the concrete covers. The column stub was created using a mesh of 8×8×7 element layers of the

Solid 65 element. The specimens were assumed to be supported on their four sides, which accurately represented the experimental configuration. The steel reinforcement bars and GFRP gratings were modeled as two node Link 8 elements, assuming a full bond with the concrete elements. All gratings' positions and sizes explored in the experiment were accounted for by the model meshing. In addition, the position of the top and bottom steel reinforcement layers, the vertical reinforcement, and the column stirrups were taken into account.

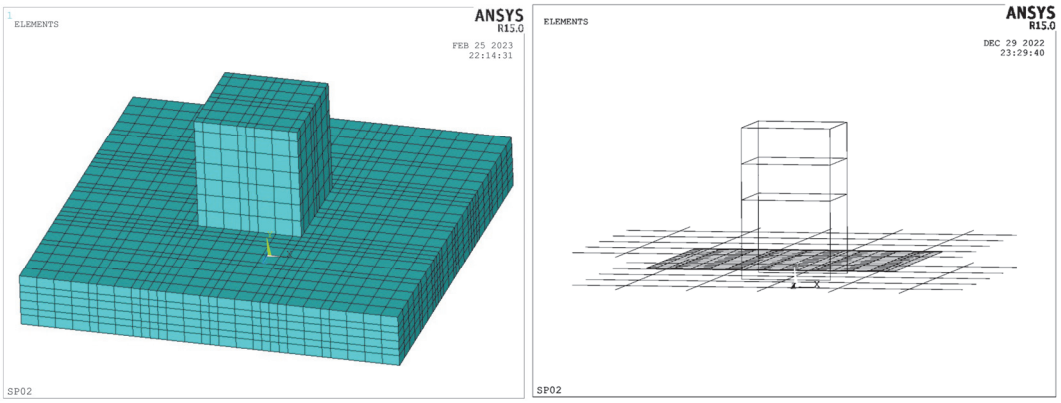

Figure 12: Idealization of concrete, reinforcement steel bars, and GFRP gratings for specimen SP02 (as an example)

RESULTS AND DISCUSSION

Analysis of the experimental results

Tab. 2 shows the experimental results: (1) first crack load, (2) failure load, (3) deflection at failure load, (4) concrete strain at failure, (5) steel strain at failure, (6) GFRP gratings strain at failure, and (7) toughness. Tab. 3 compares the test results to those of the control specimen SP01. Fig. 13 shows the effects of the studied variables on the load-deflection curves. Fig. 14 displays the first crack and failure loads for all tested specimens, whereas Figs. 15, 16 and 17 represent the bottom reinforcement, top surface concrete, and grating strains for all specimens at failure load. Fig. 18 represents the toughness of all tested specimens, showing that the use of gratings increased toughness in all cases compared to the control specimen SP01 without gratings. Specimens with GFRP gratings exhibited a greater failure load and a wider punched failure surface compared to specimen SP01 without GFRP gratings. Fig. 19 illustrates the failure modes of all the tested specimens.

Specimen Number	P_{cr} (kN)	P_f (kN)	Δ_f (mm)	ε_{cf} (10^{-3})	ε_{sf} (10^{-3})	ε_{gf} (10^{-3})			T kN/mm
						Top	Middle	Bottom	
SP01	100.47	275.62	12.39	2.28	2.20	N.A.	N.A.	N.A.	1962.76
SP02	110.27	300.52	13.98	2.04	2.32	N.A.	2.78	N.A.	2212.60
SP03	110.14	327.81	13.48	2.49	2.08	N.A.	N.A.	1.88	2251.67
SP04	110.38	331.90	13.27	2.25	1.93	2.34	N.A.	N.A.	2318.58
SP05	110.08	324.74	13.32	2.32	2.23	2.00	N.A.	1.63	2157.82
SP06	111.54	351.87	13.18	2.42	2.29	N.A.	1.96	N.A.	2377.21
SP07	110.76	332.58	14.52	2.29	2.42	N.A.	2.95	N.A.	2697.67

Table 2: Experimental test results.

Specimen Number	$P_{cr}/P_{cr\ SP01}$ (%)	$P_f/P_{f\ SP01}$ (%)	$\Delta_f/\Delta_{f\ SP01}$ (%)	$\varepsilon_{cf}/\varepsilon_{cf\ SP01}$ (%)	$\varepsilon_{sf}/\varepsilon_{sf\ SP01}$ (%)	T/T_{SP01} (%)
SP01	100.00	100.00	100.00	100.00	100.00	100.00
SP02	109.75	109.03	112.90	89.35	105.35	112.73
SP03	109.62	118.94	108.85	108.95	94.79	114.72
SP04	109.86	120.42	107.11	98.37	87.88	118.13
SP05	109.57	117.82	107.53	101.55	101.61	109.94
SP06	111.02	127.67	106.43	105.81	104.02	121.12
SP07	110.24	120.67	117.20	100.21	110.16	137.44

Table 3: Experimental test results compared to the control specimen SP01.

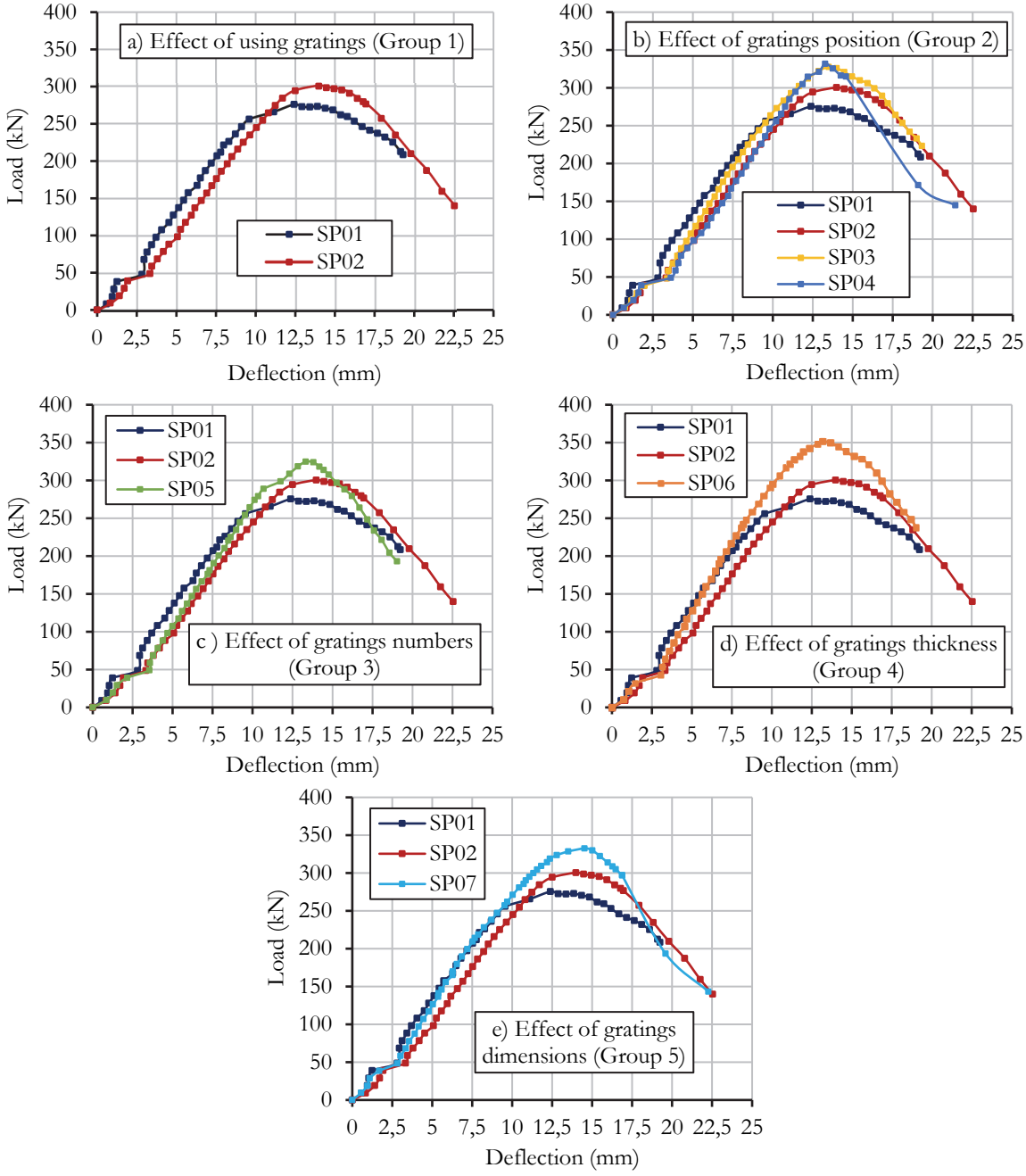

Figure 13: The effects of the studied variables on the load-deflection curves.

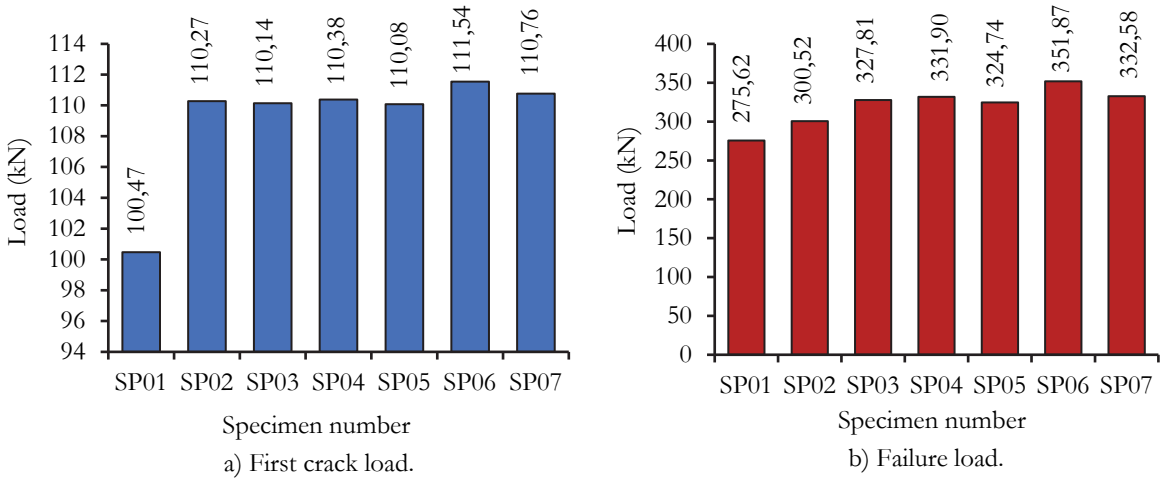

Figure 14: First crack and failure loads for all tested specimens.

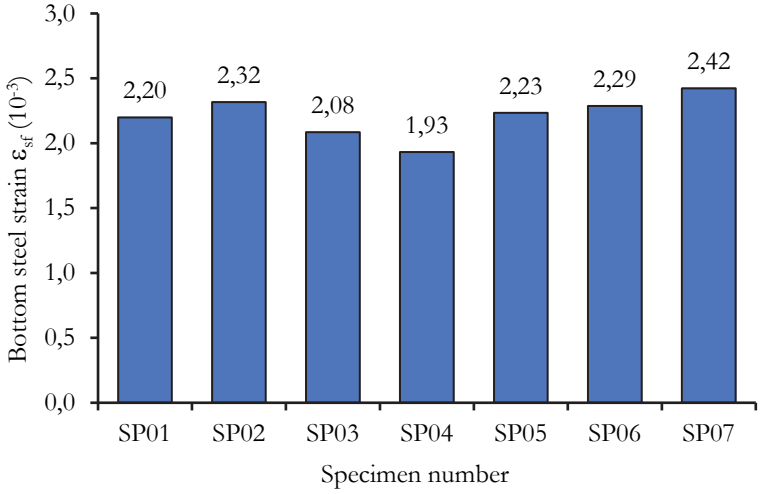

Figure 15: Bottom steel reinforcement strain for all specimens at failure load.

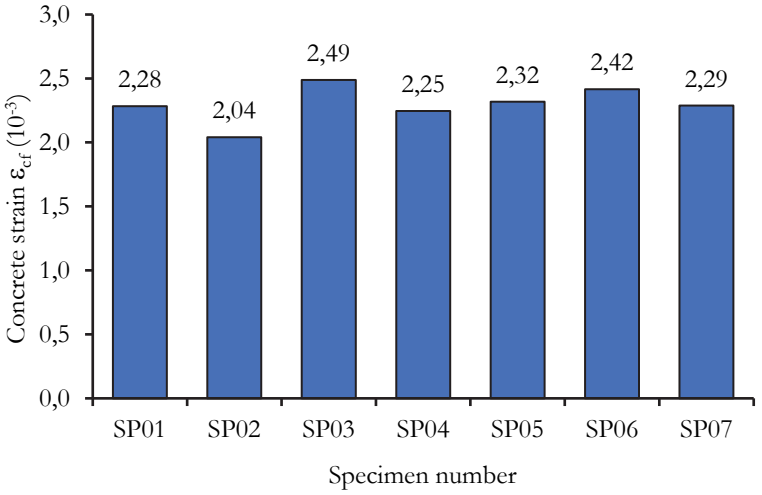

Figure 16: Concrete strain for all specimens at failure load.

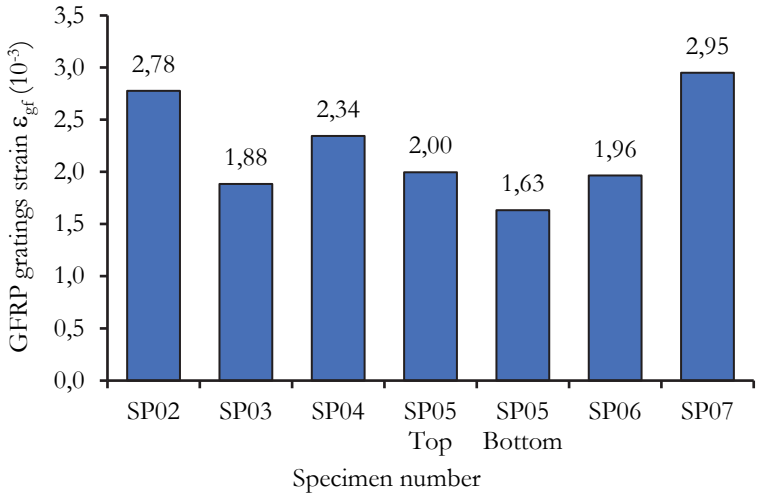

Figure 17: Gratings strain for all tested specimens at failure load.

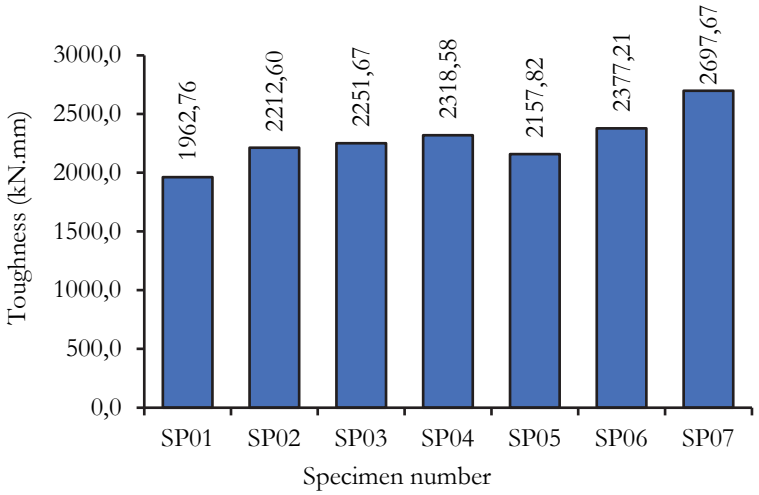

Figure 18: Toughness for all tested specimens.

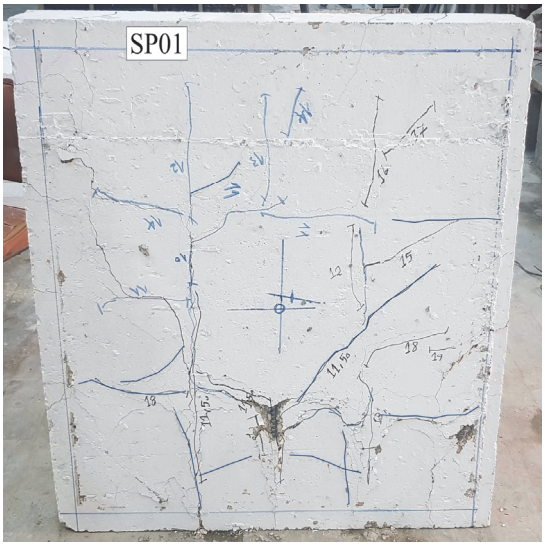

a) Specimen SP01

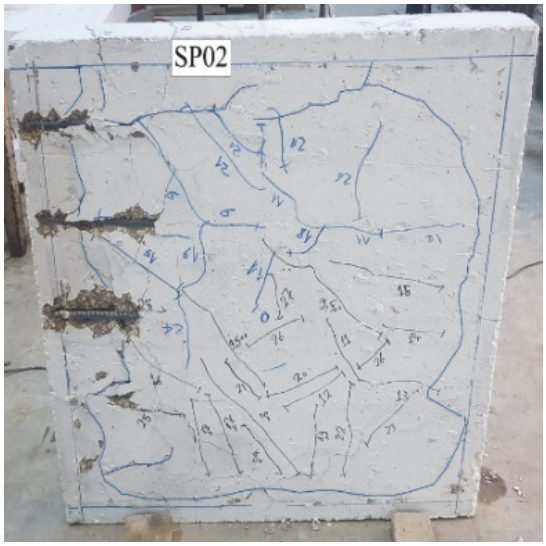

b) Specimen SP02

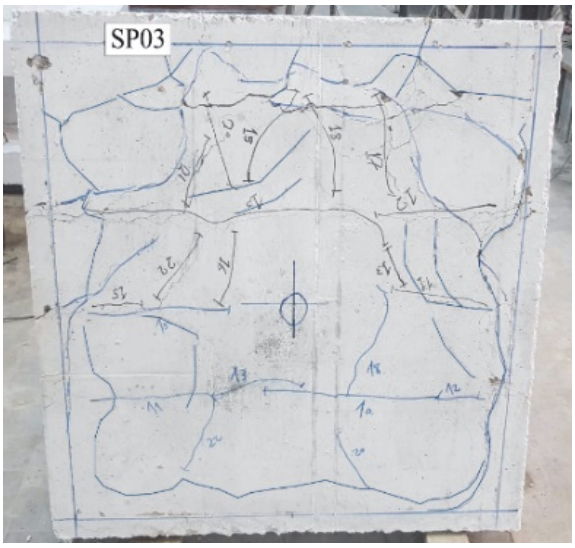

c) Specimen SP03

d) Specimen SP04

e) Specimen SP05

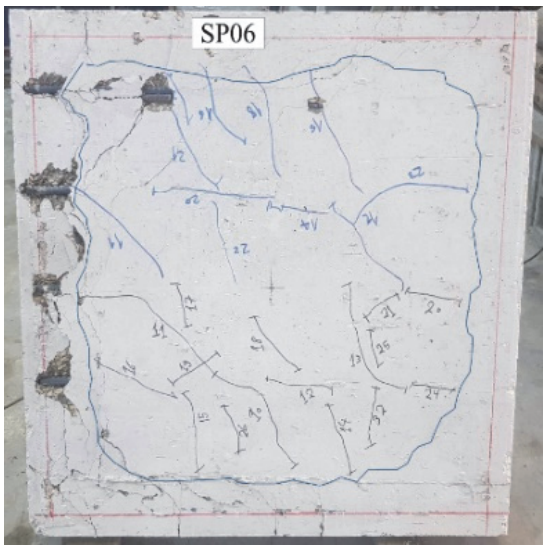

f) Specimen SP06

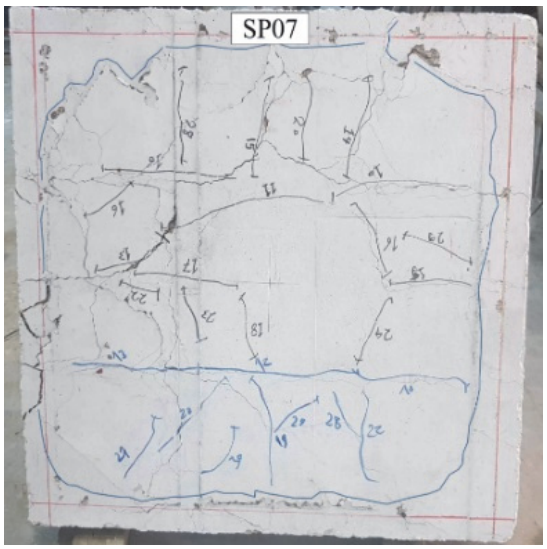

g) Specimen SP07

Figure 19: Failure modes of all tested specimens

As shown in Tab. 3 and Fig. 14(b), the integration of the GFRP gratings into the slab thickness of the tested specimens enhanced the failure load for all specimens by varying percentages. Compared to the control specimen SP01 without gratings, the presence of GFRP gratings of dimensions 700×700×15 mm at the mid-slab thickness of specimen SP02 in group (1) increased the failure load by 9.03%. For group (2), changing the position of the gratings to the bottom of specimen SP03 and the top of specimen SP04 increased the failure load by 18.94% and 20.42%, respectively. Increasing the number of GFRP gratings in a group (3) with dimensions 700×700×15 mm to two gratings attached to the top and the bottom reinforcement layers of the specimen SP05 increased the failure load by 17.82%. For group (4), increasing the GFRP gratings thickness to 38 mm for specimen SP06, with the same dimensions as 700×700 mm integrated into the mid-slab thickness, improved the failure load by 27.67%. Finally, for group 5, increasing the size of the gratings in the specimen SP07 installed at the mid-slab thickness with dimensions of 800×800×15 mm increased the failure load by 20.67%.

As shown in Fig. 15, the specimen SP07 with GFRP grating dimensions of 800×800×15 mm at the mid-slab thickness exhibited the maximum bottom steel strain. However, the specimen SP04 with grating dimensions of 700×700×15 mm, located at the top of the slab thickness, exhibited the lowest bottom steel strain, revealing the effect of grating position and size in confirming a more ductile mode of failure. Compared to the control specimen SP01, the strain reduction observed for specimen SP04 was 12.12%. However, the bottom steel strain of specimens SP05, SP06, and SP07 increased by 1.61%, 4.02%, and 10.16%, respectively, compared to specimen SP01.

From Fig. 16, the maximum concrete strain measured for specimen SP03 was 0.00249, while the minimum concrete strain measured for specimen SP02 was 0.00204. Existing GFRP grating decreased concrete strain by 10.65% when compared to the control specimen SP01 without grating. The concrete strain increased by 8.95% for the bottom grating throughout the slab thickness (specimen SP03), whereas it decreased slightly for the top position (specimen SP04) compared to the control specimen SP01. Increasing the number, thickness, and dimensions of the GFRP grating of specimens SP05, SP06, and SP07 had a marginally greater effect than that observed for the control specimen SP01.

The maximum gratings strain exhibited by specimen SP07 with grating dimensions of 800×800×15 mm, which is located at the mid-slab thickness, with a value of 0.00295, displays the effect of grating dimensions on the creation of the ductile behavior. Referring to Fig. 17, the grating strains of all specimens with a thickness of 15 mm and 38 mm didn't exceed the maximum grating strain at failure of 0.0033 and 0.0053, respectively, as determined by the experimental load-bearing test as shown in Fig. 7. For specimen SP05 with two grating layers, the minimum grating strain was observed in the top gratings attached to the top layer of the steel reinforcement.

Fig. 18 illustrates that the presence of gratings in specimen SP02 increased the toughness by 12.73% compared to specimen SP01 without gratings. The effect of gratings position enhanced the toughness by 14.72% and 18.13% for specimens SP03 and SP04, respectively, in comparison to control specimen SP01. Doubling the number of gratings in specimen SP05 enhanced the toughness by 9.94%, which revealed a detrimental effect on the ductility behavior. For specimen SP06, increasing the thickness of the gratings resulted in a 21.12% increase in toughness. Furthermore, increasing the dimensions of the gratings resulted in a significant improvement of 37.44% in toughness.

Comparison of numerical results

The numerical results from the "ANSYS 15" [24] program are consistent with the experimental results. Tab. 4 indicates that the discrepancy between the experimental and numerical results for the failure loads is within an acceptable range of 1.0% to 8.0%, with an average value and standard deviation of 1.04 and 0.03, respectively. Fig. 20 shows the experimental and numerical load–deflection curves for all tested specimens. Fig. 21 illustrates the numerical crack pattern for SP01 and SP02 specimens (as examples), whereas Fig. 22 clarifies the experimental and numerical ultimate loads for all specimens.

PARAMETRIC STUDY

An extensive parametric study has been performed using the proposed general-purpose computer package "ANSYS V.15" [24]. The examined parameters are (1) the concrete compressive strength (f_c'), (2) the steel reinforcement yield strength (f_y), (3) the main steel reinforcement ratio (μ), (4) the secondary steel reinforcement ratio (μ'), (5) column dimensions, (6) slab thickness, (7) concrete cover, (8) gratings thickness, (9) gratings dimension, (10) gratings position through the slab thickness, and (11) numbers of gratings. The model of a square flat slab with GFRP gratings investigated throughout the present parametric study has been selected such that its dimensions and properties are within practical limits, as shown in Fig. 23. The results are compared to the corresponding case of a control model with GFRP

gratings. The dimension of the control reinforced concrete slab was taken 2000×2000 mm, and the thickness was assumed to be 250 mm. The column dimensions were 400×400 mm with a height 750 mm.

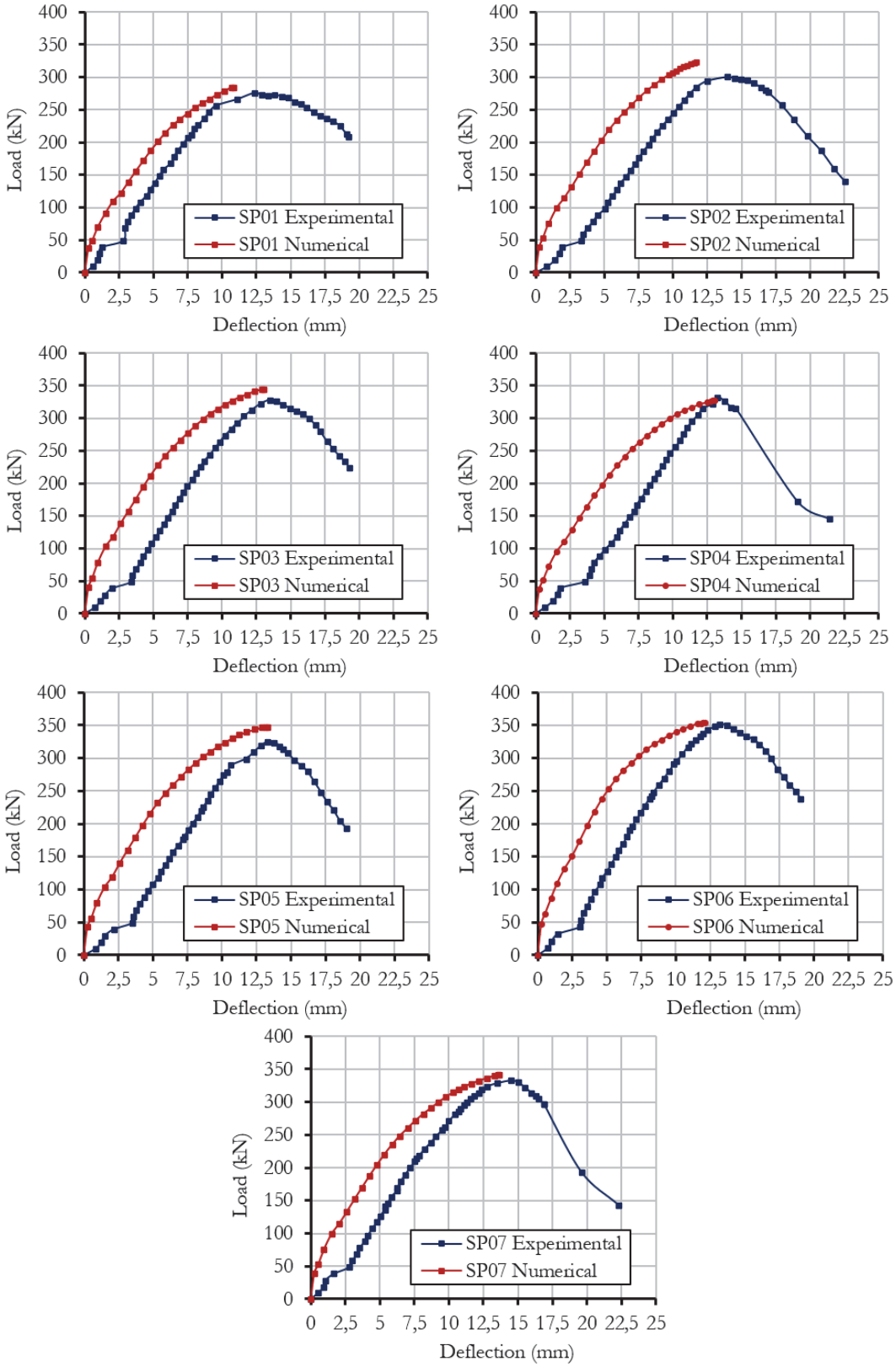

Figure 20: Experimental and numerical load–deflection curves for all tested specimens.

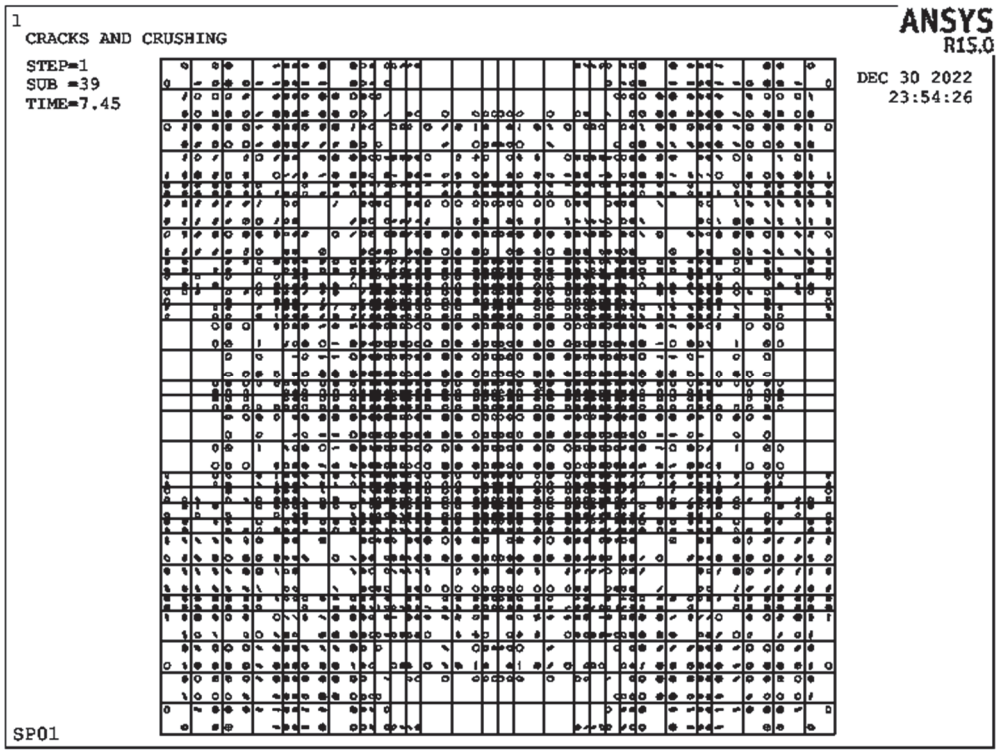

Specimen SP01

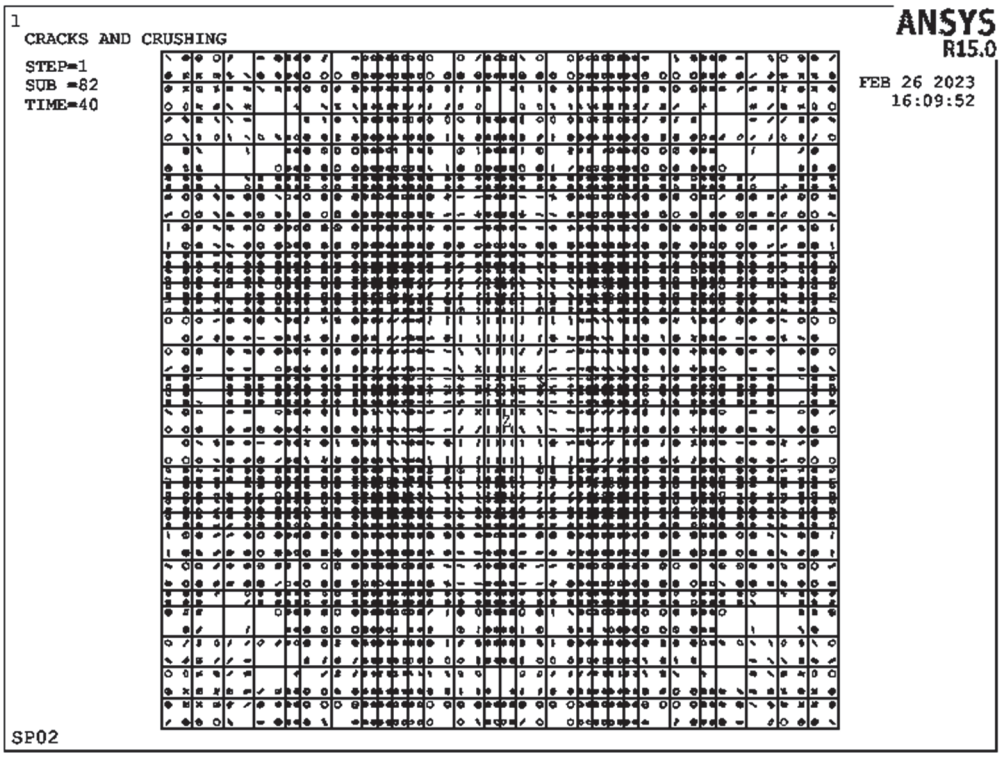

Specimen SP02

Figure 21: Numerical crack pattern for specimens SP01 and SP02 (as samples).

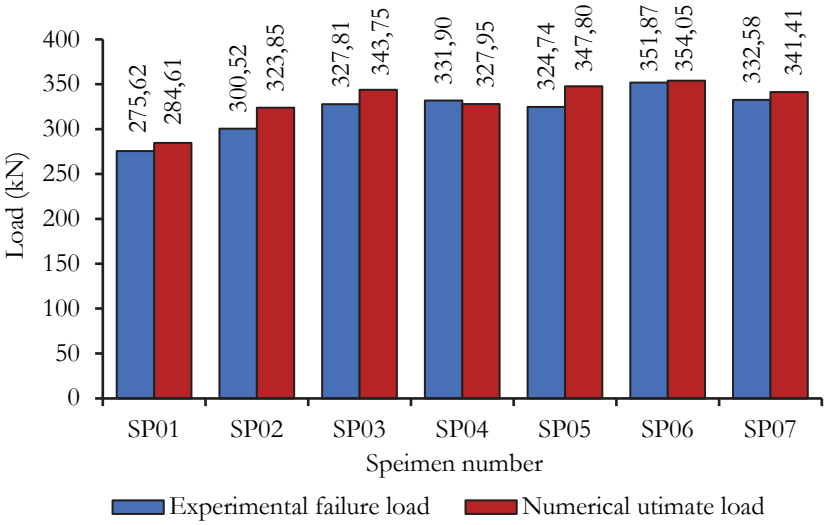

Figure 22: Experimental and numerical ultimate loads for all specimens.

Specimen Number	Experimental results			NLFEA results			NLFEA / Exp.		
	First crack load P_{cr} (kN)	Failure load P_f (kN)	Deflection at failure load $\Delta_{f\,exp}$ (mm)	First crack load N_{cr} (kN)	Ultimate load N_u (kN)	Deflection at the ultimate load $\Delta_{u\,num}$ (mm)	N_{cr} / P_{cr}	N_u / P_f	$\Delta_{u\,num}$/ $\Delta_{f\,exp}$
SP01	100.47	275.62	12.39	70.35	284.61	10.84	0.70	1.03	0.87
SP02	110.27	300.52	13.98	75.37	323.85	11.72	0.68	1.08	0.84
SP03	110.14	327.81	13.48	78.83	343.75	13.03	0.72	1.05	0.97
SP04	110.38	331.90	13.27	72.87	327.95	13.03	0.66	0.99	0.98
SP05	110.08	324.74	13.32	80.36	347.80	13.33	0.73	1.07	1.00
SP06	111.54	351.87	13.18	86.65	354.05	12.08	0.78	1.01	0.92
SP07	110.76	332.58	14.52	75.54	341.41	13.66	0.68	1.03	0.94
Mean value							0.71	1.04	0.93
Standard deviation							0.04	0.03	0.06
C.O.V.							0.05	0.03	0.06

Table 4: Comparison of test results with NLFEA from ANSYS.

For the control specimen, the steel reinforcement ratio on the tension side was assumed to be 0.35 of the maximum slab reinforcement ratio (μ_{max}), which is uniformly spaced using a mesh of 11 Φ 16 as a bottom reinforcement and 11 Φ 12 as a top secondary reinforcement mesh. The column was reinforced by 8 Φ 16 with stirrups 10 mm in diameter and 100 mm spacing. The concrete compressive strength (f_c') was taken at 25 MPa, while the steel reinforcement yield strength (f_y) was taken at 400 MPa. The GFRP grating dimensions used are 1000×1000×15 mm at the mid-slab thickness. Figs. 23 and 24 show the control model's dimensions and reinforcement details.

The range of the studied parameters

To carry out the parametric study, the concrete compressive strength (f_c') has been investigated using the following values: 25, 30, and 35 MPa. Reinforcement yield strength (f_y) was chosen as 400, 500, and 600 MPa. The slab thickness was varied (250, 300, and 350 mm) to simulate the actual thicknesses used in most typical buildings. The dimensions of the concrete slab were kept constant at 2000×2000 mm, while the column dimensions were varied (400×400, 400×500, and 400×600 mm). For main reinforcement, the ratio μ was taken as 0.35, 0.50, and 0.70 μ_{max}, where μ_{max} is the maximum reinforcement ratio. Also, for the secondary reinforcement, the ratio μ' was taken at 0.20, 0.15, and 0.25 μ_{max}. The concrete cover thickness was considered to be 20, 30, and 50 mm. The GFRP grating dimensions were 1000×1000, 1200×1200, and 1400×1400 mm, while the thickness of the gratings was chosen at 15, 30, and 38 mm. The grating's position through the slab thickness

was assumed at the middle, top, and bottom, and finally, the number of gratings was taken as one layer at the middle, one at the top, one at bottom, and three at the middle, top, and the bottom. All the studied specimens are considered subject to a static displacement applied vertically at the top in the center of the column. The considered variables in the parametric study are shown in Tab. 5.

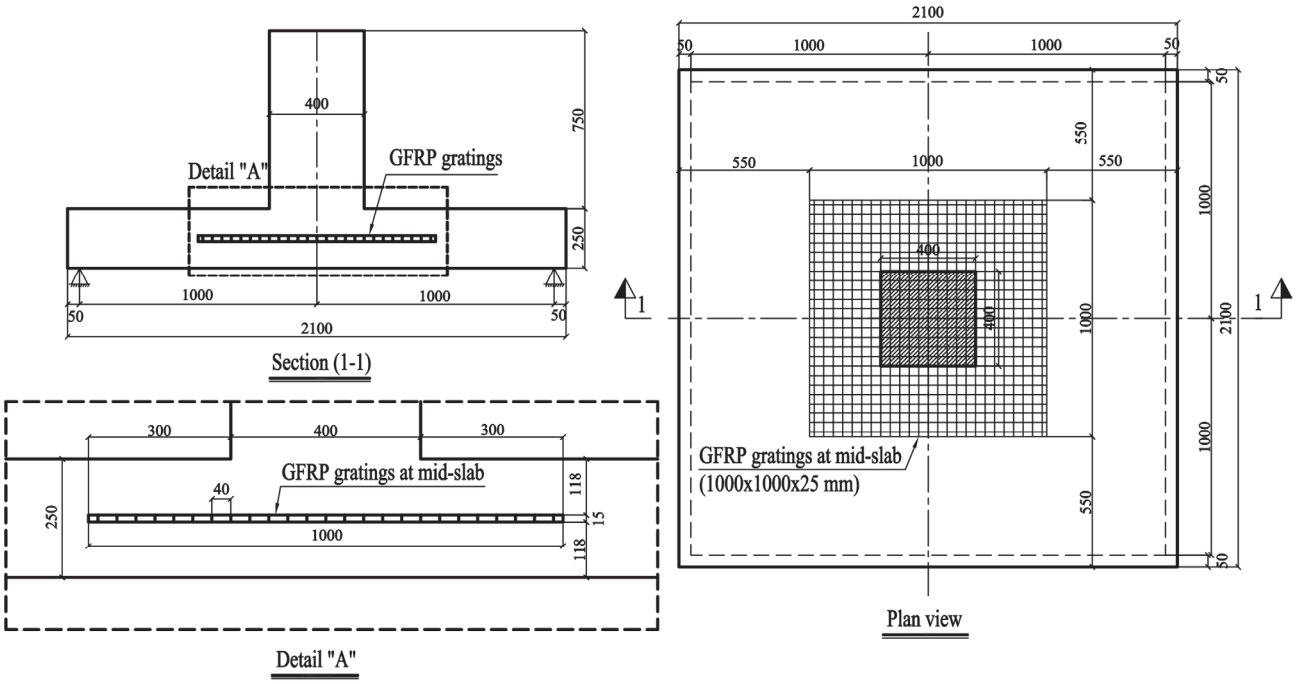

Figure 23: Typical details of the control specimen for the parametric study.

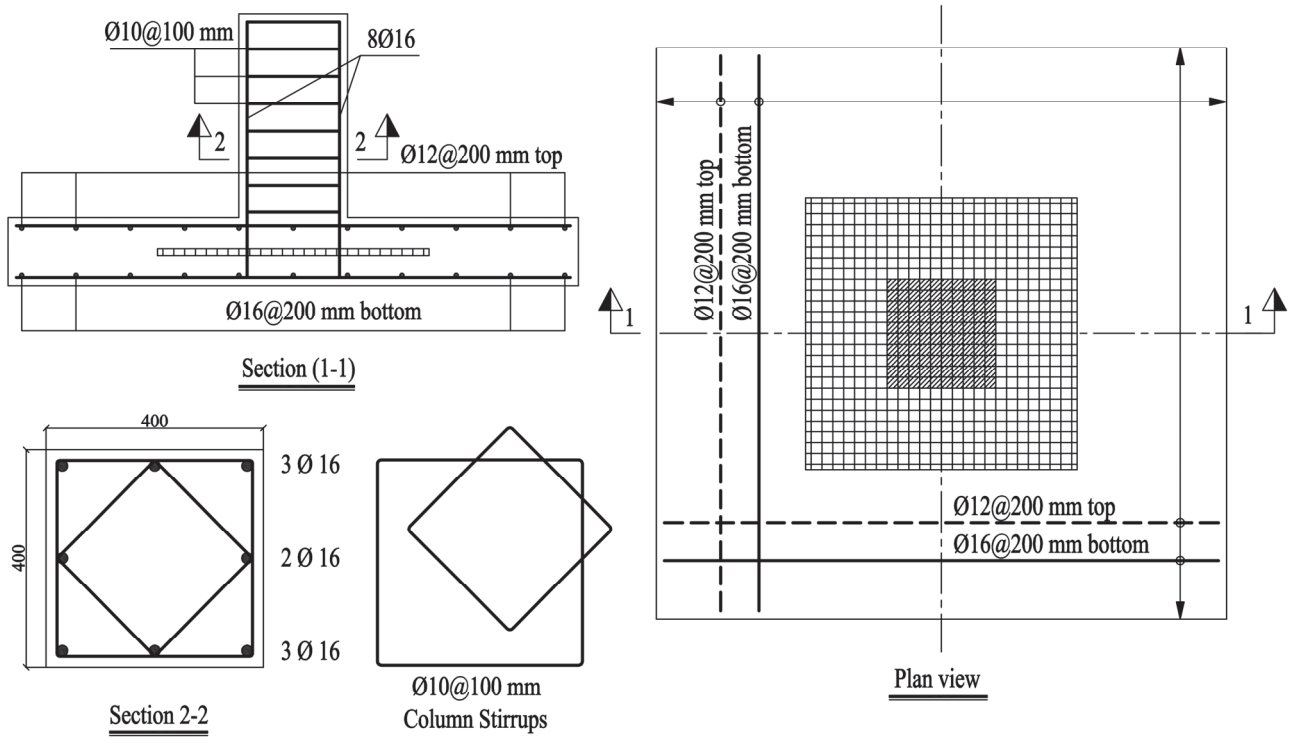

Figure 24: Typical reinforcement details of the control specimen for the parametric study.

Studied parameters													
Group number	Model number	f_c' (MPa)	f_y (MPa)	Slab thickness t_s (mm)	Column dimensions (mm)	μ / μ_{max}	μ' / μ_{max}	Concrete cover (mm)	Gratings thickness(mm)	Gratings dimensions (mm)	Gratings position	Gratings number	Notes
CM	SCM	25	400	250	400x400	0.35	0.20	30	15	1000x1000	Middle	1	Control model (CM)
1	SM01	**30**	400	250	400x400	0.35	0.20	30	15	1000x1000	Middle	1	Effect of f_c'
	SM02	**35**	400	250	400x400	0.35	0.20	30	15	1000x1000	Middle	1	
2	SM03	25	**500**	250	400x400	0.35	0.20	30	15	1000x1000	Middle	1	Effect of f_y
	SM04	25	**600**	250	400x400	0.35	0.20	30	15	1000x1000	Middle	1	
3	SM05	25	400	**300**	400x400	0.35	0.20	30	15	1000x1000	Middle	1	Effect of slab thickness
	SM06	25	400	**350**	400x400	0.35	0.20	30	15	1000x1000	Middle	1	
4	SM07	25	400	250	**400x500**	0.35	0.20	30	15	1000x1000	Middle	1	Effect of column dimensions
	SM08	25	400	250	**400x600**	0.35	0.20	30	15	1000x1000	Middle	1	
5	SM09	25	400	250	400x400	**0.50**	0.20	30	15	1000x1000	Middle	1	Effect of main steel ratio/μ_{max}
	SM10	25	400	250	400x400	**0.70**	0.20	30	15	1000x1000	Middle	1	
6	SM11	25	400	250	400x400	0.35	**0.15**	30	15	1000x1000	Middle	1	Effect of secondary steel ratio/μ_{max}
	SM12	25	400	250	400x400	0.35	**0.25**	30	15	1000x1000	Middle	1	
7	SM13	25	400	250	400x400	0.35	0.20	**50**	15	1000x1000	Middle	1	Effects of concrete cover
	SM14	25	400	250	400x400	0.35	0.20	**20**	15	1000x1000	Middle	1	
8	SM15	25	400	250	400x400	0.35	0.20	30	**30**	1000x1000	Middle	1	Effect of grating thickness
	SM16	25	400	250	400x400	0.35	0.20	30	**38**	1000x1000	Middle	1	
9	SM17	25	400	250	400x400	0.35	0.20	30	15	**1200x1200**	Middle	1	Effect of grating dimensions
	SM18	25	400	250	400x400	0.35	0.20	30	15	**1400x1400**	Middle	1	
10	SM19	25	400	250	400x400	0.35	0.20	30	15	1000x1000	**Top**	1	Effect of grating position
	SM20	25	400	250	400x400	0.35	0.20	30	15	1000x1000	**Bottom**	1	
11	SM21	25	400	250	400x400	0.35	0.20	30	15	1000x1000	Top, and bottom	**2**	Effect of numbers of gratings
	SM22	25	400	250	400x400	0.35	0.20	30	15	1000x1000	Top, middle and Bottom	**3**	

Table 5: Parametric study program.

Analysis of the parametric study results

Tab. 6 summarizes all the results of the numerical parametric study that was conducted in this study, where all the results of the ultimate loads and the central deflection at the ultimate load were compared with the results of the control specimen. It is established from Tab. 6 that the concrete compressive strength has a significant impact on the punching shear capacity of flat slabs reinforced with GFRP gratings. Increasing the concrete compressive strength increases the failure load by 15.63% and 31.96%, respectively, for specimens that have a concrete compressive strength of 30 and 35 MPa compared to the control model with a concrete compressive strength of 25 MPa.

The ultimate load increased by 6.29% and 11.54% when using steel reinforcement with f_y of 500 MPa and 600 MPa, respectively, compared to the control model with f_y of 400 MPa.

A significant and noticeable effect of the slab thickness was found on the ultimate load of the slab, where the load increased by 28.32% and 65.10% for specimens SM05 and SM06, respectively, due to an increase in the slab thickness of 20% and 40% compared to the control specimen.

There was an increase in ultimate load of 8.18% and 13.77% for specimens SM07 and SM08, respectively, when the column dimensions increased by 25% and 50%, respectively, compared to the control specimen.

An increase in the ultimate loads was 8.50% for SM09 ($\mu = 0.50\ \mu_{max}$) and 21.85% for SM10 ($\mu = 0.70\ \mu_{max}$) compared to the control specimen SCM with $\mu = 0.35\ \mu_{max}$.

Compared to the control model, the enhancement achieved was insignificant due to increasing the secondary reinforcement ratio, where the ultimate load increased by 5.84% for SM12, while a slight change was detected at 1.76% for SM11.

Compared to the control specimen SCM (concrete cover = 30 mm), the ultimate load was found to be decreased by 4.26% for specimen SM13 with a concrete cover of 50 mm and improved by 3.88% for specimen SM14 with a concrete cover of 20 mm due to increasing the slab effective depth.

Relative to the control model, specimen SM15 had two gratings of 15 mm each (total thickness 30 mm), and specimen SM16 had a thickness of 38 mm, both resulting in a minor increase in ultimate load of 5.14% and 7.22%, respectively.

Compared to the control model, the ultimate load enhancement was achieved by increasing the grating dimensions, where the increases were 5.71% and 11.92% for specimens SM17 and SM18, respectively.

The effect of the GFRP grating position was studied using specimens SM19 and SM20 at the top and bottom, respectively, compared to the control specimen SCM with gratings at mid-slab thickness. The results show a negligible increase in ultimate load at 1.63% and 3.39%, respectively. The central deflection of SM19 and SM20 has increased by 12.60% and 2.01%, respectively. The results demonstrated that the position of the gratings has an insignificant effect on the overall performance of the slab.

In comparison to the control specimen SCM, the results of specimen SM21 with two gratings at the upper and lower steel reinforcement and specimen SM22 with three gratings at the higher and lower steel layers, as well as at the mid-slab thickness, showed that the ultimate load increased by 5.51% and 5.87% for the two specimens, respectively. As a result, increasing the number of grating layers from two to three had no significant effect on the ultimate load.

COMPARISON WITH CODE PROVISIONS

The various building codes provide design provisions for punching shear strength using empirical processes derived from studies on normal-strength concrete slabs, such as ECP 203 2018 [17], ACI 318-2019 [18], EN 1992-1-1-2004 [27], BS 8110-97 [28], and AS 3600-2009 [29].

The comparison of experimental and analytical results for estimating concrete contribution was conducted without shear reinforcement, as the GFRP grating effect is not considered to have shear punching resistance in previous codes. The codes often define the design's punching shear capacity as the product of the design's nominal shear strength of concrete and a particularly critical section's area. According to the codes, the critical section for punching shear evaluation in slabs is between the column face and twice the slab's effective depth. The experimental and analytical failure loads from different international codes for the tested slabs are compared in Tab. 7. The comparison demonstrates that predictions for punching shear differ between codes. The coefficient of variation (C.O.V.) for all codes is roughly 0.08, with the mean of the predicted/experimental load capacity ratio ranging from 0.89 to 0.98. Tab. 8 shows the comparison of the analytical results from the parametric study with those from different codes. The analysis reveals that the punching shear estimations vary significantly between code provisions. Superlative results were found from EN 1992 [27], with an average predicted to the analytical ultimate load of 0.98.

Model number	Evaluated criteria		Numerical ultimate load		Comments
	Variable	Value	Ultimate load P_u (kN)	P_u/P_u SCM (-)	
SCM		25	690.11	1.000	Control model
SM01	f_c' (MPa)	30	797.95	1.156	
SM02		35	910.66	1.320	
SCM		400	690.11	1.000	Control model
SM03	f_y (MPa)	500	733.51	1.063	
SM04		600	769.75	1.115	
SCM		250	690.11	1.000	Control model
SM05	Slab thickness t_s (mm)	300	885.51	1.283	
SM06		350	1139.38	1.651	
SCM		400x400	690.11	1.000	Control model
SM07	Column dimensions (mm)	400x500	746.54	1.082	
SM08		400x600	785.11	1.138	
SCM		0.35	690.11	1.000	Control model
SM09	μ/μ_{max}	0.50	748.78	1.085	
SM10		0.70	840.91	1.219	
SM11		0.15	677.98	0.982	
SCM	μ'/μ_{max}	0.20	690.11	1.000	Control model
SM12		0.25	730.40	1.058	
SM13		50	660.70	0.957	
SCM	Concrete cover (mm)	30	690.11	1.000	Control model
SM14		20	716.87	1.039	
SCM		15	690.11	1.000	Control model
SM15	Gratings thickness (mm)	30	725.60	1.051	
SM16		38	739.95	1.072	
SCM		1000x1000	690.11	1.000	Control model
SM17	Gratings dimensions (mm)	1200x1200	729.48	1.057	
SM18		1400x1400	772.37	1.119	
SCM		Middle	690.11	1.000	Control model
SM19	Gratings position	Top	701.35	1.016	
SM20		Bottom	713.49	1.034	
SCM		1	690.11	1.000	Control model
SM21	Gratings number	2	728.11	1.055	
SM22		3	730.64	1.059	

Table 6: Parametric study program.

Specimen No.	Exp. ultimate load: P_u (kN)	Codes predicted ultimate load: V (kN)									
		ECP 203-2018 V_{ECP} (kN)	V_{ECP}/P_u	ACI 318-2019 V_{ACI} (kN)	V_{ACI}/P_u	BS 8110-1997 V_{BS} (kN)	V_{BS}/P_u	EN 1992 V_{EN} (kN)	V_{EN}/P_u	AS 3600-2009 V_{AS} (kN)	V_{AS}/P_u
SP01	275.62	312.09	1.13	291.51	1.05	286.64	1.04	285.73	1.03	300.34	1.09
SP02	300.52	312.09	1.04	291.51	0.97	286.64	0.95	285.73	0.95	300.34	1.00
SP03	327.81	312.09	0.95	291.51	0.89	286.64	0.87	285.73	0.87	300.34	0.92
SP04	331.90	312.09	0.94	291.51	0.88	286.64	0.86	285.73	0.86	300.34	0.90
SP05	324.74	312.09	0.96	291.51	0.89	286.64	0.88	285.73	0.87	300.34	0.92
SP06	351.87	312.09	0.89	291.51	0.83	286.64	0.81	285.73	0.81	300.34	0.85
SP07	332.58	312.09	0.94	291.51	0.88	286.64	0.86	285.73	0.86	300.34	0.90
Mean value			0.98		0.91		0.90		0.89		0.94
Standard deviation			0.08		0.07		0.07		0.07		0.08
C.O.V			0.08		0.08		0.08		0.08		0.08

Table 7: Comparisons of experimental results with the predictions of building codes for the tested slabs.

Specimen No.	Num. ultimate load: N_u (kN)	Codes predicted ultimate load: V (kN)									
		ECP 203-2018 V_{ECP} (kN)	V_{ECP}/N_u	ACI 318-2019 V_{ACI} (kN)	V_{ACI}/N_u	BS 8110-1997 V_{BS} (kN)	V_{BS}/N_u	EN 1992 V_{EN} (kN)	V_{EN}/N_u	AS 3600-2009 V_{AS} (kN)	V_{AS}/N_u
SCM	690.11	844.63	1.22	788.93	1.14	658.16	0.95	708.17	1.03	812.84	1.18
SM01	797.95	927.52	1.16	867.23	1.09	701.01	0.88	754.28	0.95	893.51	1.12
SM02	910.66	927.52	1.02	1005.69	1.10	773.77	0.85	832.58	0.91	1036.17	1.14
SM03	733.51	844.63	1.15	788.93	1.08	658.16	0.90	708.17	0.97	812.84	1.11
SM04	769.75	844.63	1.10	788.93	1.02	658.16	0.86	708.17	0.92	812.84	1.06
SM05	885.51	1120.19	1.27	1046.32	1.18	782.90	0.88	894.02	1.01	1078.02	1.22
SM06	1139.38	1426.71	1.25	1332.62	1.17	908.42	0.80	1093.73	0.96	1373.00	1.21
SM07	746.54	912.75	1.22	852.55	1.14	678.70	0.91	735.84	0.99	878.39	1.18
SM08	785.11	980.86	1.25	916.18	1.17	698.93	0.89	763.50	0.97	943.94	1.20
SM09	748.78	844.63	1.13	788.93	1.05	689.66	0.92	742.07	0.99	812.84	1.09
SM10	840.91	844.63	1.00	788.93	0.94	788.38	0.94	848.29	1.01	812.84	0.97
SM11	677.98	844.63	1.25	788.93	1.16	658.16	0.97	708.17	1.04	812.84	1.20
SM12	730.40	844.63	1.16	788.93	1.08	658.16	0.90	708.17	0.97	812.84	1.11
SM13	660.70	743.08	1.12	694.07	1.05	608.43	0.92	637.88	0.97	715.11	1.08
SM14	716.87	897.27	1.25	838.09	1.17	683.05	0.95	744.20	1.04	863.49	1.20
SM15	725.60	844.63	1.16	788.93	1.09	658.16	0.91	708.17	0.98	812.84	1.12
SM16	739.95	844.63	1.14	788.93	1.07	658.16	0.89	708.17	0.96	812.84	1.10
SM17	729.48	844.63	1.16	788.93	1.08	658.16	0.90	708.17	0.97	812.84	1.11
SM18	772.37	844.63	1.09	788.93	1.02	658.16	0.85	708.17	0.92	812.84	1.05
SM19	701.35	844.63	1.20	788.93	1.12	658.16	0.94	708.17	1.01	812.84	1.16
SM20	713.49	844.63	1.18	788.93	1.11	658.16	0.92	708.17	0.99	812.84	1.14
SM21	728.11	844.63	1.16	788.93	1.08	658.16	0.90	708.17	0.97	812.84	1.12
SM22	730.64	844.63	1.16	788.93	1.08	658.16	0.90	708.17	0.97	812.84	1.11
Mean value			1.17		1.10		0.90		0.98		1.13
Standard deviation			0.07		0.06		0.04		0.04		0.06
C.O.V			0.06		0.05		0.04		0.04		0.05

Table 8: Comparisons of experimental results with the predictions of building codes for the tested slabs.

COMPARATIVE ANALYSIS WITH PREVIOUS RESEARCH

In the realm of failure load, prior studies, such as those by Swamy and Ali [1], Zhang et al. [4], and Abdulrahman et al. [8], have explored the impact of various FRP reinforcements on punching shear capacity. Swamy and Ali's [1] use of fibers throughout the slab and comparative tests with steel bars demonstrate increased ultimate punching shear loads. In comparison, the current study introduces molded GFRP gratings, resulting in a notable improvement in failure load ranging from 9.03% to 27.67%. This signifies a distinct contribution, showcasing the effectiveness of GFRP gratings in enhancing punching shear resistance in flat slab-column connections.

Regarding failure mode, studies like Kim and Lee [11] emphasize the transition from brittle punching to flexure with GFRP reinforcement. The current research is in contrast to this trend, as all tested specimens, including those with GFRP gratings, failed in a punching shear mode with brittleness. However, the specimens with GFRP gratings exhibited a larger punched failure surface, indicating that the GFRP reinforcement influenced the failure mode, showcasing a unique characteristic not extensively discussed in prior literature.

In terms of studied parameters, many previous works, including Hemzah et al. [9] and Said et al. [10], have explored variations in slab shape, reinforcement types, and double-layer effects. In comparison, the current study introduces parameters specific to GFRP gratings, such as location, number, thickness, and size. This targeted investigation provides detailed insights into the nuanced effects of GFRP grating characteristics on punching shear resistance, complementing the broader parameters studied in the existing literature.

Code provisions play a crucial role in design, and Stuart et al. [7] underline variations in code accuracy for FRP-reinforced concrete. The current study aligns with this observation, noting that predictions based on EN 1992-1-1-2004 were more conservative compared to ECP 203-2018, AS 3600-2009, and ACI 318-2019. Additionally, the BS 8110-97 code yielded results with a mean predicted-to-analytical ultimate load ratio of 0.90, showcasing the importance of considering code provisions in the design process.

Numerical studies have been a focus in various works, and Mu and Meyer [3] emphasize the experimental validation of analytical models. The current study employs a nonlinear finite element approach using "ANSYS V.15" software, producing superior results for crack patterns, load-carrying capacity, and load-deflection response. The numerical results align closely with experimental findings, with ultimate failure loads ranging from 99% to 108% of the experimental failure load, demonstrating the reliability and accuracy of the numerical model.

Analytical studies often consider factors like concrete compressive strength and reinforcement properties. In this regard, Dimitrios et al. [5] predict the ultimate strength of FRP-reinforced structural elements. The current study extends this by showcasing the considerable influence of GFRP grating dimensions, position, and number on the analytical ultimate load. It emphasizes that increasing compressive strength, yield strength of tension reinforcement, slab thickness, and column dimensions positively impact the analytical ultimate load, contributing additional insights for practical design considerations.

In summary, while prior literature provides a foundation for understanding FRP reinforcement in concrete structures, the current study, centered on GFRP gratings, introduces distinctive contributions in failure load, failure mode, studied parameters, code provisions, numerical, and analytical studies. These comparisons underscore the unique insights offered by the current research in the field of punching shear-strengthening methods.

CONCLUSIONS

The study introduces a novel reinforcing system employing GFRP gratings to enhance punching shear resistance in RC flat slabs. Experimental tests on seven specimens showcase the effectiveness of this novel reinforcing system. Nonlinear Finite Element Analysis (NLFEA) using ANSYS affirms the system's efficiency. The results exhibit a strong correlation between numerical simulations and experimental outcomes. Systematic exploration of key parameters through NLFEA compares the novel reinforcing system's results to recent code provisions.

Research outcomes

The specimens equipped with GFRP grating displayed greater punching perimeters compared to the control specimen without gratings. Additionally, crack patterns were comparable for all the provided GFRP grating specimens. All tested specimens failed in a punching shear failure mode with brittleness, and the specimens with GFRP gratings had a larger punched failure surface than the specimens without GFRP grating.

Specimens provided with the proposed gratings exhibited an increase in the failure load. This improvement varied from 9.03% to 27.67%, according to the values of the studied parameters. The addition of GFRP grating at the mid-slab thickness increased the failure load by 9.03%. Using gratings at the bottom and the top of the slab increased the failure load by 18.94% and 20.42%, respectively, compared to the control specimen without gratings. The use of two layers of gratings at the bottom and the top increased the failure load by 17.82% compared to the control specimen without gratings.

The failure load increased by 17.09% when increasing the GFRP grating thickness from 15 mm to 38 mm located at the mid-slab thickness while maintaining the same GFRP grating dimensions. The failure load increased by 27.67% when increasing the dimensions of the grating layer located at the mid-slab thickness by 15%. Maximum strains of 0.0025, 0.0024, and 0.0029 were recorded in the concrete in compression, bottom steel reinforcement, and GFRP gratings of the tested specimens, respectively, which means that the steel reinforcement yielded while the GFRP gratings didn't fail. Furthermore, the use of gratings increased the toughness of the tested specimens, which ranged from 9.94% to 37.44% according to the values of the studied parameters.

The employment of the nonlinear finite element approach using "ANSYS V.15" software produced superior results for crack patterns, load carrying capacity, and load-deflection response. The numerical results using the "ANSYS V.15" software showed that the ultimate failure loads ranged from 99% to 108% of the experimental failure load.

The analytical load-carrying capacity of the RC flat slabs using GFRP gratings was considerably affected by the concrete compressive strength. An increase of 15.63% and 31.96% in the ultimate load was obtained due to increasing the compressive strength by 20% and 40%, respectively. Increasing the yield strength of the main tension reinforcement from 400 MPa to 500 MPa and 600 MPa slightly affected the ultimate load, where the predicted ultimate load was enhanced by about 6.29% and 11.54%, respectively.

The predicted analytical ultimate load was significantly improved by 28.32% and 64.10% when increasing the slab thickness by 20% and 40%, respectively. The enhancement of the predicted ultimate load was about 8.18% and 13.77% when increasing column dimensions by 25% and 50%, respectively. Increasing the tension reinforcement steel ratio had a significant effect on the punching resistance, where the analytical ultimate load of the slabs provided with 0.50 μ_{max} and 0.70 μ_{max} was 108.50% and 121.85%, respectively, compared to that of the control slab, which was provided with 0.35 μ_{max}, where μ_{max} is the maximum ratio of the steel reinforcement area to the concrete section area.

Increasing the secondary reinforcement compression steel ratio from 0.15 μ_{max} to 0.20 μ_{max} and 0.25 μ_{max} resulted in insignificant enhancements of 1.8% and 7.7% in the predicted ultimate load. The increase of the concrete cover by 50% and 250% decreased the predicted ultimate load by 3.7% and 7.8%, respectively, due to the decrease in the slab's effective depth.

The analytical ultimate load improved by 5.1% and 7.2%, respectively, when the thickness of the grating was increased from 15 mm to 30 mm and 38 mm. The analytical ultimate load enhancement was achieved by increasing the grating dimensions by 20% and 40%, where the increases were 5.71% and 11.92%, respectively. A negligible effect of the GFRP grating position was noticed due to changing the position of the GFRP gratings from top to bottom of the slab thickness, where an increase of 1.63% and 3.39%, respectively, in the analytical load was found compared to the specimen with GFRP grating at the midpoint of the slab. The increase in the analytical ultimate load due to the increases in grating number from two to three was insignificant, where the analytical ultimate load improved by 5.51% and 5.87%, respectively, compared to the specimen with one layer of GFRP grating.

In comparison to the code provisions without the effect of shear reinforcement, the EN 1992-1-1-2004 code achieved superior underestimated (conservative) analytical results with a mean predicted to analytical ultimate load ratio of 0.98, while the ECP 203-2018, AS 3600-2009, and ACI 318-2019 codes produced overestimated (unconservative) results with analytical to predicted numerical ultimate load ratios of 1.17, 1.13, and 1.10, respectively. On the other hand, good results of the BS 8110-97 code yielded a mean predicted to analytical ultimate load ratio of 0.90. The mean of the predicted and experimental failure load ratios ranges from 0.89 to 0.98 for all codes, with a standard deviation of 0.07.

Recommendations for future research

In light of the findings from this study, several recommendations for future research endeavors are proposed to further enhance the understanding and application of reinforced concrete (RC) flat slabs using fiber-reinforced polymers (FRP) gratings. Firstly, exploring alternative FRP materials, such as carbon-fiber-reinforced polymers (CFRP), could offer valuable insights into their effectiveness in enhancing punching shear resistance. Comparative studies between GFRP and CFRP gratings may reveal the unique characteristics and potential advantages of each material. This study contributes to a more comprehensive understanding of GFRP and CFRP grating applicability to structural elements.

Furthermore, varying the spacing of molded gratings presents an intriguing area for exploration. Modifying the spacing between gratings may influence the structural behavior and load-carrying capacity of RC flat slabs. A systematic study on the impact of different grating spacings on punching shear resistance could lead to recommendations for optimal spacing configurations. This study enables designers to tailor reinforcement strategies based on specific project requirements.
Additionally, investigating the use of pultruded gratings as a reinforcement system represents an avenue for future research. Pultruded gratings, known for their high strength and durability, could offer distinct mechanical properties compared to molded gratings. An examination of their performance in punching shear resistance in RC flat slabs under various loading conditions would provide valuable data for engineers and researchers seeking optimal FRP reinforcement solutions.

REFERENCES

[1] Swamy, R. N., and Ali, S. A. R. (1982). Punching shear behavior of reinforced slab-column connections made with steel fiber concrete. ACI Structural Journal, 79(5), pp. 392-406. DOI: 10.14359/10917.

[2] Ospina, C. E., Alexander, S. D. B., and Cheng, J. J. R. (2003). Punching of two-way concrete slabs with fiber-reinforced polymer reinforcing bars or grids. ACI Structural Journal, (100) 5, pp. 589-598. DOI: 10.14359/12800.

[3] Mu, B., and Meyer, C. (2003). Bending and punching the shear strength of fiber-reinforced glass concrete slabs. ACI Structural Journal, (100)2, pp. 127-132. DOI: 10.14359/12552.

[4] Zhang, B., Masmoudi, R., and Benmokrane, B. (2004). The behavior of one-way concrete slabs reinforced with CFRP grid reinforcements. Construction and Building Materials, 18, pp. 625-635. DOI: 10.1016/j.conbuildmat.2004.04.007.

[5] Dimitrios, D., Theodorakopoulos, H., and Swamy, N. (2007). Analytical model to predict punching shear strength of FRP-reinforced concrete flat slabs. ACI Structural Journal, (104), 3, pp. 257-266. DOI: 10.14359/18615.

[6] Esfahani, M. R., Kianoush, M. R., and Moradi, A. R. (2007). Punching shear strength of interior slab column connections strengthened with carbon fiber-reinforced polymer sheets. Engineering Structures, (31) 7, pp. 1535-1542. DOI: 10.1016/j.engstruct.2009.02.021.

[7] Stuart, V., and Cunningham, L.S. (2017). FRP-reinforced concrete slabs: A comparative design study. Proceedings of the Institution of Civil Engineers Structures and Buildings, (170) 8, pp. 581-602. DOI:10.1680/jstbu.16.00055

[8] Abdulrahman B. Q., Wu Z., and Cunningham L. S. (2017). Experimental and numerical investigation into strengthening flat slabs at corner columns with externally bonded CFRP. Construction and Building Materials, (139), pp. 132-147. DOI: 10.1016/j.conbuildmat.2017.02.056

[9] Hemzah, S. A., Al-Obaidi, S., and Salim, T. (2019). Punching shear model for normal and high-strength concrete slabs reinforced with CFRP or steel bars. Jordan Journal of Civil Engineering, (13) 2, pp. 250-268.

[10] Said, M., Adam, M.A., Arafa, A.E., and Moatasem, A. (2020). Improvement of the punching shear strength of reinforced lightweight concrete flat slabs using different strengthening techniques. Journal of Building Engineering, 32, 101749. DOI: 10.1016/j.jobe.2020.101749.

[11] Kim, M. S., and Lee, Y. H. (2021). Punching the shear strength of reinforced concrete flat plates with GFRP vertical grids. Applied Sciences, (11) 6, DOI: 10.3390/app11062736.

[12] Bank, L.C., Xi, Z., and Munley, E. (1992). Tests of full-size pultruded FRP gratings reinforced concrete bridge decks. Conference Proceedings of ASCE, Materials Engineering Congress, New York, pp. 618-631.

[13] Bank, L.C., Frostig, Y., and A. Shapira (1997). Three-dimensional FRP grating cages for concrete beams. ACI Structural Journal, (94) 6, pp. 643-652. DOI: 10.14359/9724.

[14] Biddah A., (2006). Structural reinforcement of bridge decks using pultruded GFRP gratings. Composite Structures, 74, pp. 80-88. DOI: 10.1016/j.compstruct.2005.03.016.

[15] Devender, B., Purushotham, A. and Reddy, V. (2013). Experimental tests on GFRP gratings were constructed for mechanical properties and chemical resistance. IOSR Journal of Mechanical and Civil Engineering, (8) 6, pp. 34-39.

[16] Gattesco, N., Dilena, M., and Boem, I. (2019). Experimental and numerical study on the bending performances of glass FRP-molded gratings. Influence of restraining conditions and cover plates, Composite Structures, 223, p. 110967. DOI: 10.1016/j.compstruct.2019.110967.

[17] ECP Committee (2018). Egyptian Code for Design and Construction of Concrete Structures (ECP 203-2018). Housing and Building National Research Center, Cairo, Egypt.

[18] ACI Committee 318 (2020). Building Code Requirements for Structural Concrete (ACI 318-19). An ACI Standard, Commentary on Building Code Requirements for Structural Concrete (ACI 318R-19), American Concrete Institute.

[19] ASTM, A370-17 (2006). Standard Test Method and Definition for Mechanical Testing of Steel Product. West Conshohocken, PA, USA.

[20] ASTM, C39/C39M-21 (2021). Standard Test. Method for Compressive Strength of Cylindrical Concrete Specimens, ASTM International, West Conshohocken, PA, USA.
[21] ASTM, C496/C496M-17 (2017). Standard test method for splitting tensile strength of cylindrical concrete specimens. ASTM International, West Conshohocken, PA, USA.
[22] ECP 208-2005 (2005). Egyptian Code for the Use of Fiber Reinforced Polymers (FRP) in the Construction Fields. Egyptian Housing and Building National Research Center.
[23] ASTM D790-02 (2002). Standard test methods for the flexural properties of unreinforced and reinforced plastics and electrical insulating materials. ASTM International, West Conshohocken, PA, USA.
[24] Manual, F.L.U.E.N.T. (2012). ANSYS Release Version 15.0. User's Guide.
[25] Martinez, S., Nilson, A. H., and Slate, F. (1984). Spirally-reinforced high-strength concrete columns. ACI Structural Journal, (81) 5, pp. 431-442. DOI: 10.14359/10693.
[26] Mahmoud, A.M. (2015). Finite element implementation of punching shear behaviors in shear-reinforced flat slabs. Ain Shams Engineering Journal, 6(3), pp. 735-754. DOI: 10.1016/j.asej.2014.12.015
[27] Eurocode 2, EN 1992-1-1 (2004). Design of concrete structures-Part 1-1: General Rules and Rules for Buildings.
[28] Standard, BS 8110 (1997). Structural use of concrete: Part 1: Code of Practice for Design and Construction. British Standard Institute, London.
[29] AS3600-09 (2009). Concrete structures, Standards Association of Australia.

NOMENCLATURE

P_{cr}	Experimental first crack load;
N_{cr}	Numerical first crack load;
P_f	Experimental failure load;
N_u	Numerical ultimate load;
$\Delta_{f\,exp}$	Experimental deflection at mid-span at failure load;
$\Delta_{u\,num}$	Numerical deflection at mid-span at ultimate load;
ε_{cf}	Concrete compressive strain at failure load;
ε_{sf}	Bottom reinforcement steel strain at failure load;
ε_{gf}	GFRP gratings strain at failure load;
T	Toughness which is the ability to adsorb deformations up to failure and equals the area under the load-deflection curve up to failure;
f_c'	The average concrete cylinder compressive strength; and
f_y	Reinforcement yield strength.